

Mechanisms of the Vertical Secular Heating of a Stellar Disk

N. Ya. Sotnikova (nsot@astro.spbu.ru)
S. A. Rodionov (seger@astro.spbu.ru)

*Astronomical Institute, St. Petersburg State University,
Universitetskii pr. 28, Petrodvorets, St. Petersburg, 198904 Russia*

Abstract

We investigate the nonlinear growth stages of bending instability in stellar disks with exponential radial density profiles. We found that the unstable modes are global (the wavelengths are larger than the disk scale lengths) and that the instability saturation level is much higher than that following from a linear criterion. The instability saturation time scales are of the order of one billion years or more. For this reason, the bending instability can play an important role in the secular heating of a stellar disk in the z direction. In an extensive series of numerical N -body simulations with a high spatial resolution, we were able to scan in detail the space of key parameters (the initial disk thickness z_0 , the Toomre parameter Q , and the ratio of dark halo mass to disk mass M_h/M_d). We revealed three distinct mechanisms of disk heating in the z direction: bending instability of the entire disk, bending instability of the bar, and heating on vertical inhomogeneities in the distribution of stellar matter.

STELLAR RELAXATION IN THE DISKS OF SPIRAL GALAXIES

According to the theory of stellar evolution, the correlation between the spectral types of stars in the solar neighborhood and their kinematic parameters found more than half a century ago (Parenago 1950) is the reflection of another correlation between the stellar age and the random velocity dispersion (for a review of the currently available data, see, e.g., Fuchs et al. 2000). The latter correlation has the following pattern: the velocity dispersion for old stars is, on average, larger than that for young stars. All stars are born with a small spread in random velocities (about 5–10 km s⁻¹). In this case, the increase in the velocity dispersion with time (dynamic heating) is the reflection of a random scattering of stars (continuous or occasional) by massive objects or large-scale density inhomogeneities.

Two pioneering studies (Spitzer and Schwarzschild 1951, 1953), in which large gaseous structures discovered twenty years later as giant molecular clouds (GMCs) from CO observations were postulated as scattering objects, were based on this idea. Subsequently, other relaxation mechanisms, for example, interaction with close satellites, were also suggested. The latter mechanism relies on observational data, according to which the disks of galaxies in interacting systems are a factor of 1.5 or 2 thicker than the disks of isolated galaxies (Reshetnikov and Combes 1997). Its efficiency is confirmed by numerical simulations (Walker et al. 1999; Velazquez and White 1999).

For isolated galaxies, apart from scattering by GMCs, the heating on inhomogeneities in the distribution of stellar matter that arise during the development of internal instabilities in the disk itself is commonly considered. The heating can be produced by transient spiral arms or a growing bar and by bending instability.

In suggesting a particular dynamic heating mechanism, the following two well-established observational facts should be borne in mind.

(1) The stellar velocity dispersion depends on time as $\sigma_{\text{tot}} \propto t^\alpha$, where σ_{tot} is the three-dimensional velocity dispersion and $\alpha \approx 0.33 - 0.5$ (Fuchs et al. 2000; Binney et al. 2000).

(2) The ratio of the vertical and radial stellar velocity dispersions is $\sigma_z/\sigma_R < 1$.

The second fact requires an explanation. It is well known that in an equilibrium axisymmetric galaxy in the absence of the third integral of motion, σ_z and σ_R must be equal at a given point of the disk (see, e.g., Saslaw 1989). Observational data indicate that this is not the case. The σ_z/σ_R ratio for stars in the solar neighborhood does not depend on their spectral type (and, hence, on their age) and is $\sigma_z/\sigma_R = 0.53 \pm 0.07$ (see, e.g., Dehnen and Binney 1998). Until recently, no similar data have been available for external galaxies. At present, this ratio is known for two more nearby galaxies¹: $\sigma_z/\sigma_R = 0.70 \pm 0.19$ for NGC 488 (morphological type Sb) (Gerssen et al. 1997) and $\sigma_z/\sigma_R = 0.85 \pm 0.1$ for NGC 2985 (morphological type Sab) (Gerssen et al. 2000); i.e., it increases as one passes to earlier-type galaxies.

Spitzer and Schwarzschild (1951, 1953) showed that when stars are scattered by GMCs, the stellar velocity dispersion increases as $\sigma_{\text{tot}} \propto t^{1/3}$; i.e., the exponent corresponds to the lower limit of this quantity, which is still in agreement with observational data. If, however, we take into account the fact that the GMCs are confined in a thin layer and the stars lie outside this layer most of the time, then the efficiency of the relaxation mechanism associated with GMCs becomes even lower: $\sigma_{\text{tot}} \propto t^{0.25}$ (Lacey 1984). At the same time, GMCs are capable of effectively converting the energy of random motions in the disk plane into the energy of random motions in the perpendicular direction. Lacey (1984) found that when stars are scattered by GMCs, a ratio $\sigma_z/\sigma_R \approx 0.8$ is rapidly established. This ratio is much larger than the value observed for the solar neighborhood, although it is close to that obtained for the galaxy NGC 2985. However, no CO-line emission was detected for this galaxy (see, e.g., Merrifield et al. 2000).

As regards the spiral arms, numerical simulations (the first numerical results were obtained by Sellwood and Carlberg 1984) and analytical calculations (Binney and Lacey 1988; Jenkins and Binney 1990; Jenkins 1992) show good agreement between the theoretical and observational age – velocity dispersion relations. However, the following should be remembered: in the above theoretical studies, the spiral arms were assumed to effectively scatter stars only in the disk plane. Additional mechanisms are commonly invoked to convert part of the energy in the disk plane into the energy of vertical motions. The combined effect from spiral arms and GMCs yields a result that is in good agreement with observational data (Binney and Lacey 1988), but this does not rule out

¹In both cases, we give galaxy-averaged data.

other vertical disk heating mechanisms. For isolated galaxies, bending instability can serve as such a mechanism. In addition, as we show below, spiral arms are capable of producing density inhomogeneities in the z direction. The interaction of stars with these density enhancements also result in an increase of σ_z .

Here, we study in detail the nonlinear growth stages of bending instability and show that it can be responsible for the secular increase of the stellar velocity dispersion in the vertical direction.

BENDING INSTABILITY AS A MECHANISM OF THE SECULAR HEATING OF STELLAR DISKS

The Linear Theory

Stellar disks are known to be unstable against the formation of spiral arms and bars. In addition, conditions for the growth of bending instability exist in thin equilibrium disks. This instability arises in systems with highly anisotropic particle motions and is similar to the fire-hose instability in plasma.

The bending instability of an infinitely thin gravitating layer with a nonzero velocity dispersion was first investigated by Toomre (1966). Toomre is believed to have been sceptical about his results. Therefore, they were published in a barely accessible paper and only several years ago did they become widely known after their detailed presentation by Merrit and Sellwood (1994). The bending instability of flat stellar systems has been rediscovered several times. Kulsrud et al. (1971) independently obtained a result similar to that of Toomre (1966). As regards equilibrium cold disks (with a zero velocity dispersion), Hunter and Toomre (1969) showed that they (in contrast to hot disks) are stable against the growth of bending perturbations. This fact had long been misused as an argument against any astrophysical applications related to bending instability. Only in 1977 did Polyachenko and Shukhman construct an exact linear theory for a homogeneous thin layer with a nonzero stellar velocity dispersion. A more realistic model of a thin layer with the vertical density profile described by the function $\text{sech}^2(z/z_0)$ was analyzed by Araki (1985)².

Toomre (1966) was the first to derive the dispersion relation for long-wavelength ($\lambda = 2\pi/k \gg h$, where $2h$ is the layer thickness) bending perturbations

$$\omega^2 = 2\pi G\Sigma|k| - \sigma_x^2 k^2, \quad (1)$$

where Σ is the surface density of the layer stars and σ_x^2 is the velocity dispersion along a particular coordinate in the layer plane. It follows from Eq. (1) that perturbations with wavelengths $\lambda > \lambda_J \equiv \sigma_x^2/G\Sigma$ are stable, because $\omega^2 > 0$ in this range.

Short-wavelength perturbations

$$\lambda < \lambda_2 \approx h \frac{\sigma_x}{\sigma_z} = h\alpha,$$

²The presentation of the results of this analysis by Sellwood and Merritt (1994) made it accessible for a wide circle of researchers.

where

$$\alpha \equiv \frac{\sigma_x}{\sigma_z}, \quad (2)$$

is the control parameter of the bending instability, must also be stable. In this case, the time of one vertical stellar oscillation, $t_{\perp} = h/\sigma_z$, is longer than the time it takes for the star to traverse one wavelength, $t_{\parallel} = \lambda/\sigma_x$. Therefore, the star traverses a distance of several wavelengths in the time t_{\perp} . As a result, a mismatch in the coherent particle motion arises, causing the perturbation to decay. Intermediate-wavelength ($\lambda_2 < \lambda < \lambda_J$) perturbations are unstable; the bending only grows.

When $\lambda_2 = \lambda_J$, the instability region disappears and the disk becomes stable against bending perturbations of any wavelengths. The following analytical estimate is valid for the parameter α defined by formula (2) in the linear approximation (Toomre 1966; Kulsrus et al. 1971; Polyachenko and Shukhman 1977; Araki 1985):

$$\lambda_2 = \lambda_J \text{ for } \alpha = \alpha_{\text{cr}} \approx 3.0,$$

or

$$\left(\frac{\sigma_z}{\sigma_x}\right)_{\text{cr}} \approx 0.3. \quad (3)$$

The instability is completely suppressed for $\sigma_z/\sigma_x > 0.3$ and grows for $\sigma_z/\sigma_x < 0.3$.

Stars are born out of a gaseous medium and initially have low random velocities. The increase of the velocity dispersion in the radial and azimuthal directions through scattering by spiral density waves can lead to an anisotropy of the particle motions in the plane and in the vertical direction. As a result, bending instability can develop in the disk; this instability causes an increase in σ_z to the level corresponding to instability saturation and an increase in the stellardisk thickness. The linear criterion gives a low instability saturation level (3). However, as was mentioned above, $\sigma_z/\sigma_R \approx 0.5$ in the solar neighborhood. That is why Toomre was sceptical about his discovery. However, the following two things should be remembered. First, $(\sigma_z/\sigma_R)_{\text{cr}} \approx 0.3$ was obtained from a linear analysis. Numerical studies of the nonlinear growth stages of bending instability (Raha et al. 1991; Sellwood and Merritt 1994; Merrit and Sellwood 1994; and our numerical results) show that the instability is saturated at much larger σ_z/σ_R . Second, the growth rate of the instability is very low. The saturation time scales are several billion years.

For these two reasons, bending instability can play an important role in the secular disk heating in the z direction.

The Numerical Model

A high spatial resolution in the z direction is required to properly simulate the growth of bending instability in numerical simulations. In the N -body problem, this is possible only for a large number of gravitationally interacting particles. In the first numerical models, N was taken to be 100 000 (Raha et al. 1991; Sellwood and Merritt 1994; Merrit and Sellwood 1994). We used a considerably larger number of particles, $N = 300\,000 - 500\,000$, which made it possible to reach a higher resolution and to trace the evolution of the stellar disk on time scales of about 5 Gyr. In addition, our model of

a disk galaxy is much more realistic: we considered a rotating disk with an exponential density profile and assumed the existence of an additional spherical component (a dark halo). Finally, we scanned in detail the space of control parameters (see the next section) and found many of the growth features of bending instability that were overlooked both in the linear analysis and in the numerical simulations.

In our numerical simulations, we simulated the evolution of an isolated disk galaxy by using an algorithm that is based on the data structuring in the form of an hierarchical tree (Barnes and Hut 1986). Its implementation was taken from the NEMO package (<http://astro.udm.edu/nemo>; Teuben 1995). The package was adapted to personal computers and significantly expanded by including original data analysis and visualization programs.

In specifying a galaxy model, we separated two subsystems: the stellar disk and the spherically symmetric component (a dark halo). Star formation was disregarded. The disk was represented as a system of gravitating bodies with R and z density profiles, which corresponds to the observed brightness profiles for spiral galaxies:

$$\rho_d(R, z) = \frac{M_d}{4\pi h^2 z_0} \cdot \exp\left(-\frac{R}{h}\right) \cdot \operatorname{sech}^2\left(\frac{z}{z_0}\right), \quad (4)$$

where h is the exponential disk scale length, z_0 is the typical scale of density variation in the z direction, and M_d is the total disk mass.

The spherical component was described in terms of the external static potential

$$\Phi_h(r) = -\frac{v_\infty^2}{2} \ln(r^2 + a_h^2), \quad (5)$$

where a_h is the typical scale and v_∞ is the velocity of a particle on a circular orbit in this potential for $r \rightarrow \infty$ (v_∞ can be expressed in terms of the halo mass within a sphere of a given radius and the parameter a_h).

We specified the initial particle velocities (the rotation velocity and the random component) on the basis of equilibrium Jeans equations using a standard technique with a specified dependence $\sigma_R^2 \propto \Sigma(R)$, where $\Sigma(R)$ is the disk star surface density (see, e.g., Hernquist 1993).

All of the parameters specified in a numerical simulation can be divided into three groups: input parameters of the algorithm for solving the N -body problem, parameters of the initial model, and control parameters of the problem (the parameters that significantly affect the processes under consideration).

(1) Parameters of the algorithm: $\delta t = 0.5 \times 10^6$ yr (occasionally, 0.25×10^6 yr) is the integration step; $T_{\text{end}} = 3000 - 5000$ Myr is the total integration time, $\theta = 0.7$ is the parameter responsible for the accuracy of calculating the force (see, e.g., Hernquist 1987); in addition, in our computations, we took not one but the first two terms in the Laplace expansion of the potential: the monopole and quadrupole terms (Hernquist 1987); $\textit{eps} = 0.02$ kpc is the potential smoothing parameter.

(2) Parameters of the initial model: $h = 3.5$ kpc is the exponential disk scale length; $a_h = 2$ kpc is the dark-halo scale parameter; and $M_d = (4 - 8) \times 10^{10} M_\odot$ is the disk mass.

Table 1: Initial parameters of the numerical models

$M_{\text{halo}}(4h)/M_{\text{disk}}(4h)$	z_0 (kpc)	Q		
		1.5	2.0	2.2
3.0	0.1	9_1	12	
1.5	0.1	24	27_1	33
0.85	0.1	22	23	31
	0.25	28	29, 29_1	
0.6	0.1	8, 8_1	11, 11_1, 11_2, 11_3	20
	0.25	21		
	0.3		26, 26_1	
	0.4	30		
	0.5		32	

(3) Control parameters of the problem. Let us consider them in more detail.

(A) $z_0 = 0.1 - 0.5$ kpc is the initial disk halftickness (this quantity can be related to the initial velocity dispersion σ_z by assuming that the system is vertically isothermal, $\sigma_z^2 = \pi G z_0 \Sigma(R)$). Since we are concerned with the increase of the stellar velocity dispersion in the z direction, we constructed an initially thin equilibrium galaxy with a small value of z_0 . This, in turn, implies a small velocity dispersion in the z direction. Next, we observed the development of bending instability, which leads to stellar relaxation. By varying z_0 , we were able to determine the instability saturation level independent of the initial conditions.

The assumption that the system is isothermal and the dependence $\sigma_R^2 \propto \Sigma(R)$ taken from empirical considerations yields the relation $\sigma_z/\sigma_R = \text{const}$ for the initial time. The ratio σ_z/σ_R has always been lower than the value that follows from the linear criterion for bending instability. As a result, we were able to subsequently analyze the instability saturation level for various R .

(B) $Q_{8.5} = 1.5 - 2.2$ is the Toomre parameter (Toomre 1964) at $R_{\text{ref}} = 8.5$ kpc (this quantity characterizes the initial radial velocity dispersion at this radius R_{ref}). It follows from the dependence $\sigma_R^2 \propto \Sigma(R)$ that

$$Q = \sigma_R/\sigma_R^{\text{cr}} \propto \Sigma^{1/2} \frac{\kappa}{\Sigma} \propto \kappa(R) \exp(R/2h),$$

where κ is the epicyclic frequency; i.e., in contrast to σ_z/σ_R , Q is not constant for the entire disk. The function $Q(R)$ for an exponential disk has a broad maximum in the range $h < R < 3h$ (see Fig. 1 in Hernquist 1993). Specifying $R_{\text{ref}} \approx 2.5h \approx 8.5$ kpc gives the condition $Q(R) \geq Q_{8.5}$. This condition, in turn, ensures a level of stability against perturbations in the disk plane that is not lower than the level specified at R_{ref} .

Here, we were concerned with two cases:

— a large value of $Q_{8.5}$ (≈ 2.0) or, in other words, a large initial radial velocity dispersion at which the formation of a bar in the disk is suppressed; this allows the

development of bending instability to be traced in pure form (without the influence of a bar).

— a moderate value of $Q_{8.5}$ (≈ 1.5); in this case, the disk is unstable against the growth of a bar mode and we were able to investigate the influence of a bar on the relaxation in the z direction.

(C) $M_h(4h)/M_d(4h) = 0.6 - 3.0$ is the ratio of dark-halo mass to disk mass within a sphere of radius $4h$. The spherical component is a stabilizing factor during the development of bending instability; we consider its influence on the secular galaxy heating in the section entitled “Stellar Relaxation in Models...”.

For our computations, we used PC-compatible computers of the Astronomical Institute of the St. Petersburg State University. Some of the numerical simulations were carried out in cluster mode. The table gives the numbers of all of the models analyzed below³.

Results of the Numerical Simulations

We carried out a large series of stellar-dynamics simulations and studied the growth of bending instability in thin stellar disks as a function of the control parameters of the problem. Analysis of the results of our computations revealed three distinct mechanisms of stellar relaxation in the vertical direction. The following system of units is used in all of the figures that illustrate our conclusions: the unit of time is 1 Myr; the unit of velocity is 978 km s⁻¹; and the unit of length is 1 kpc.

Large-Scale Bending Instability of the Disk. The large-scale bending instability of the entire disk is the first galaxy heating mechanism. It is most typical of galaxies with low-mass spherical components that are initially hot in the plane, i.e., of galaxies in which the formation of a bar was suppressed (for bar-mode suppression mechanisms, see, e.g., the monograph of Binney and Tremaine 1987).

Below, we describe the scenario for the development of bending instability using Model 26_1 as an example. All of the key evolutionary features of the stellar disk that were shown by this model were also observed in other hot models.

If we decompose $\overline{z(R)}$ (the mean particle deviation from the $z = 0$ plane) into Fourier harmonics, $\bar{z}_m(R) = A_m \exp(-im\varphi)$, then we can calculate the amplitudes of the first three harmonics ($m = 0$ is the axisymmetric bending or, alternatively, the bell mode; $m = 1$ is the bending mode; and $m = 2$ is the saddle-type mode). The change of A_m with time describes the various bending formation stages shown in Figs. 1 and 2 (left panels). These stages are more clearly distinguished in the color two-dimensional histograms that can be found at http://www.astro.spbu.ru/staff/seger/articles/warps_2002/fig1_web.html. In these histograms, the mean disk particle deviation from the $z = 0$ plane is represented by different colors (the shades of yellow and blue indicate upward and downward deviations, respectively). We see in Figs. 1 and 2 (as in the two-dimensional histograms) that a large-scale bending is produced in the galaxy at a time $t \approx 200$ Myr. At $t \approx 400$ Myr, the

³The models with equal control parameters have different random realizations of the initial conditions — particle positions and random velocities.

bending amplitude reaches its local maximum. The bending perturbation wavelength (the radial extent) is comparable to the disk scale length. The bending is not axisymmetric; the amplitude of the zero mode, i.e., the mode with the azimuthal number $m = 0$, is small, at least less than the amplitudes of other harmonics. This relationship between the harmonic amplitudes is preserved until $t \approx 800$ Myr.

Next, a steadily growing axisymmetric bending mode ($m = 0$) is clearly revealed, while all of the still large (in amplitude) nonaxisymmetric modes ($m = 1$ and $m = 2$) are displaced to the galactic periphery. Subsequently ($t \approx 800 - 1200$ Myr), the nonaxisymmetric bending modes are gradually damped, while the axisymmetric bending reaches its maximum ($t \approx 1000$ Myr).

For the subsequent 1500 Myr of its evolution, the disk freezes in a shape similar to the shape of circles on water. A similar vertical disk structure, with box-shaped isophotes in central regions, was also observed in the numerical simulations of Sellwood and Merritt (1994) for initially hot Kuzmin – Toomre disk models and in other simulations in which the bar formation was suppressed through a large Toomre parameter Q (Patsis et al. 2002). In our computations, the amplitude of the axisymmetric bending slowly decreased and, to all appearances, the bending must subsequently disappear altogether.

Two evolutionary stages of the bending can be separated in this model: the initial stage with a nonaxisymmetric bending and the main stage with an axisymmetric bending.

Let us turn to the plot of the vertical (σ_z) and radial (σ_R) velocity dispersions against time (Fig. 3a). The value of σ_z approximately doubled in time $t = 3000$ Myr. Two times of rapid increase in the velocity dispersion σ_z can be distinguished: one at $t \approx 500$ Myr (the time the amplitude of the initial nonaxisymmetric bending reaches its maximum) and the other at $t \approx 1000 - 1200$ Myr (the time the amplitude of the main axisymmetric bending reaches its maximum). As we see, the two times of change in σ_z are closely related to the characteristic growth stages of bending instability. Such a relationship exists in all of the models without bars in which bending instability developed. Thus, we can conclude that in this model, the bending instability is responsible for the increase in σ_z ; when the bell ($m = 0$) mode appears, the energy of the random stellar velocity in the disk plane is converted most effectively into the energy of random vertical motions.

Note that the integrated quantities σ_z and σ_R calculated for the entire galaxy were used to construct the plots in Fig. 3. These quantities allow us to judge only the general run of the processes in the disk. Figure 4 shows the radial profiles of the azimuthally averaged σ_z for various times. We see that the relaxation effect is most pronounced for central regions.

In Fig. 5, the σ_z/σ_R ratio is plotted against R for several times (here, we also averaged σ_z/σ_R in concentric rings). We can conclude from our data that the saturation level of the bending instability in a region of about two exponential disk scale lengths in size (about $7 - 7.5$ kpc) is much higher than its level predicted by the linear criterion (3). For these regions, $\sigma_z/\sigma_R \approx 0.4 - 0.8$.

In Figs. 1 and 2 (right panels), the edge-on image of a model galaxy is represented by isophotes for several times. The image was vertically magnified by a factor of 4. As a result, the disk bending is clearly seen. Note

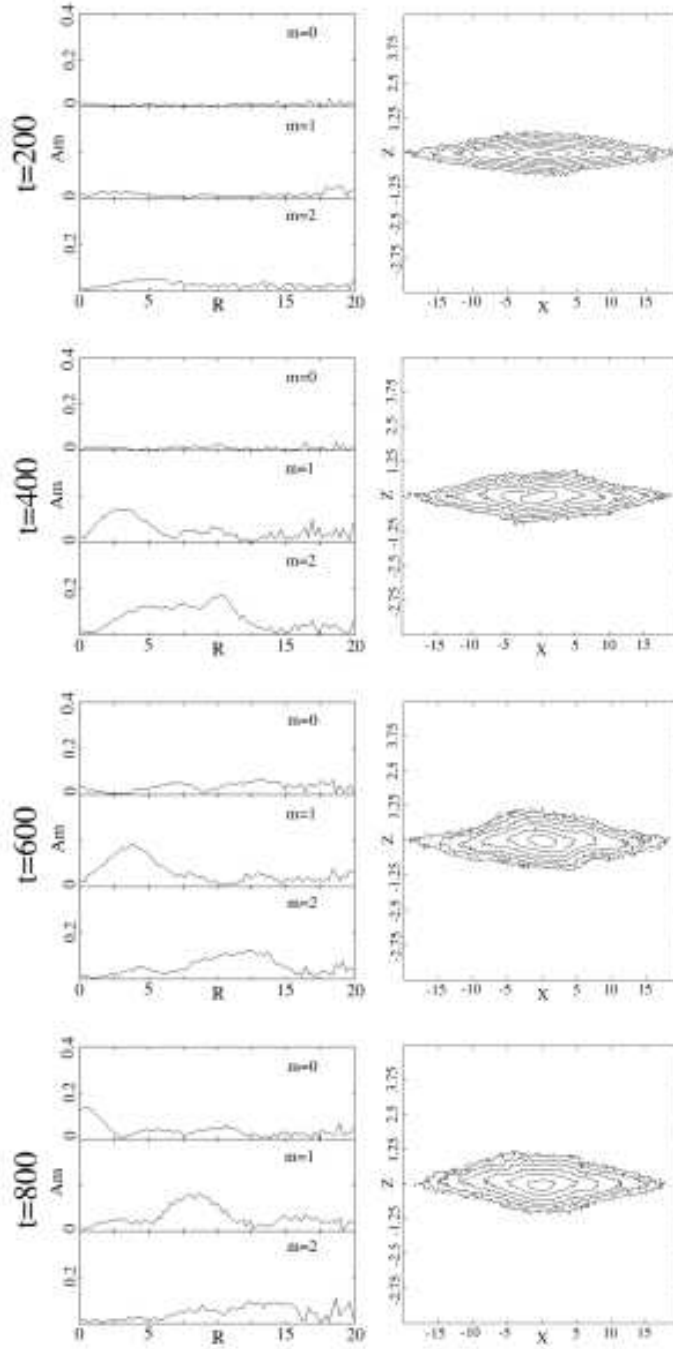


Figure 1: Model 26_1. Early evolutionary stages of the bending. The left frames: the radial distribution of the amplitude of the first three harmonics ($m = 0, 1, 2$) for the bending perturbation for several times. The right frames: an edge-on view of the galaxy — the isophotal distribution. The horizontal and vertical frame sizes are 40 and 10 kpc, respectively; i.e., **the vertical scale was increased by a factor of 4!**

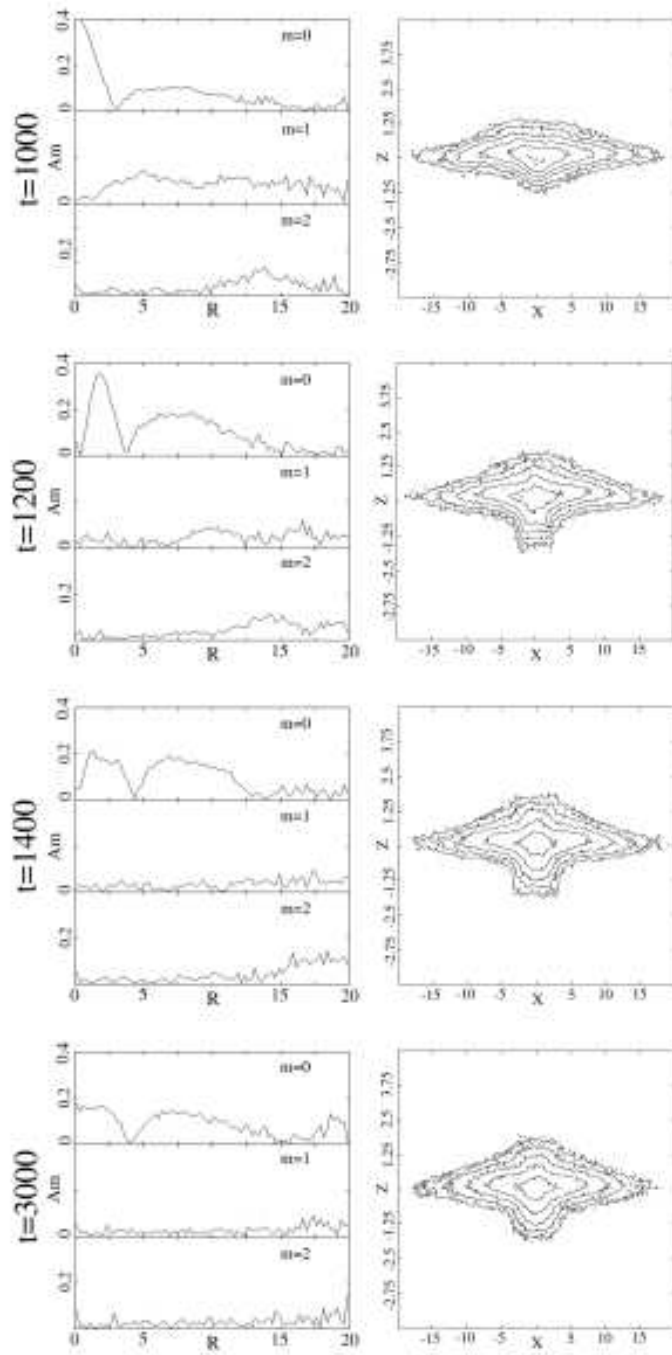


Figure 2: Model 26_1. The same as Fig. 1 for late evolutionary stages.

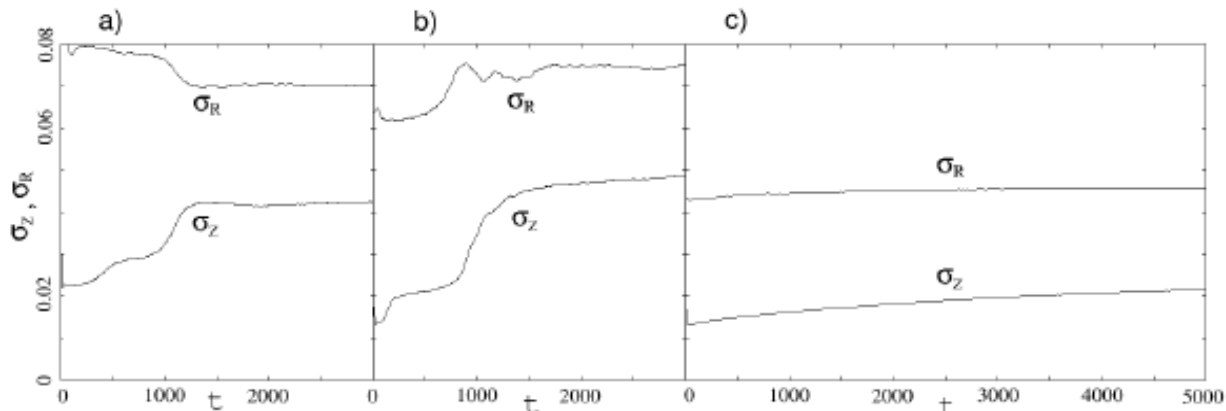


Figure 3: σ_R (upper curve) and σ_z (lower curve) versus time. The integrated quantities referred to the entire galaxy are plotted: (a) Model 26_1; (b) Model 8_1; and (c) Model 9_1.

that the galactic evolution at late stages gives rise to a family of X-shaped orbits in central regions of the disk ($t = 1200, 1400, 3000$; the left frames; the X-shaped structures are more clearly seen on the pseudoimage of the model galaxy, http://www.astro.spbu.ru/staff/seger/articles/warps_2002/fig1_web.html). The main axisymmetric bending may be saturated at a galaxy thickness at which a resonance arises between the frequencies of the stellar oscillations across the disk and in the rotation plane. This resonance can produce X-shaped orbits, which have repeatedly been observed in numerical simulations (Combes et al. 1990; Pfenninger and Friedli 1991; Patsis et al. 2002).

In other models, the initial and main bends manifested themselves differently than those in Model 26_1. The behavior of all models can be assigned to one of the following cases.

(1) Both the initial and main bends arose almost simultaneously. In the long run, only the axisymmetric bending survived. Abrupt disk heating took place at the time the bending amplitude was increasing. This scenario was observed for initially thin galaxies, i.e., for the models that started from initial conditions far from the linear saturation level. Almost all of the models with $Q_{8,5} = 2.0$ and $z_0 < 0.3$ kpc show such a pattern of evolution.

(2) The occurrences of the initial and main bends were well separated in time, as for Model 26_1 described in detail.

(3) There was no initial bending at all, while the main bending could be observed at very late evolutionary stages. This scenario is characteristic of initially thick disks, i.e., of the models that started from conditions close to the instability saturation limit. This result closely corresponds to the following theoretical result: at a given ratio of the masses of the spherical and disk components, the mode with the azimuthal number $m = 1$ becomes stable earlier than the other modes as the disk thickness increases (Fridman and Polyachenko 1984). As the disk thickness increases further, the $m = 2$ mode is ultimately saturated and the $m = 0$ mode remains at the fore. Note that the results of

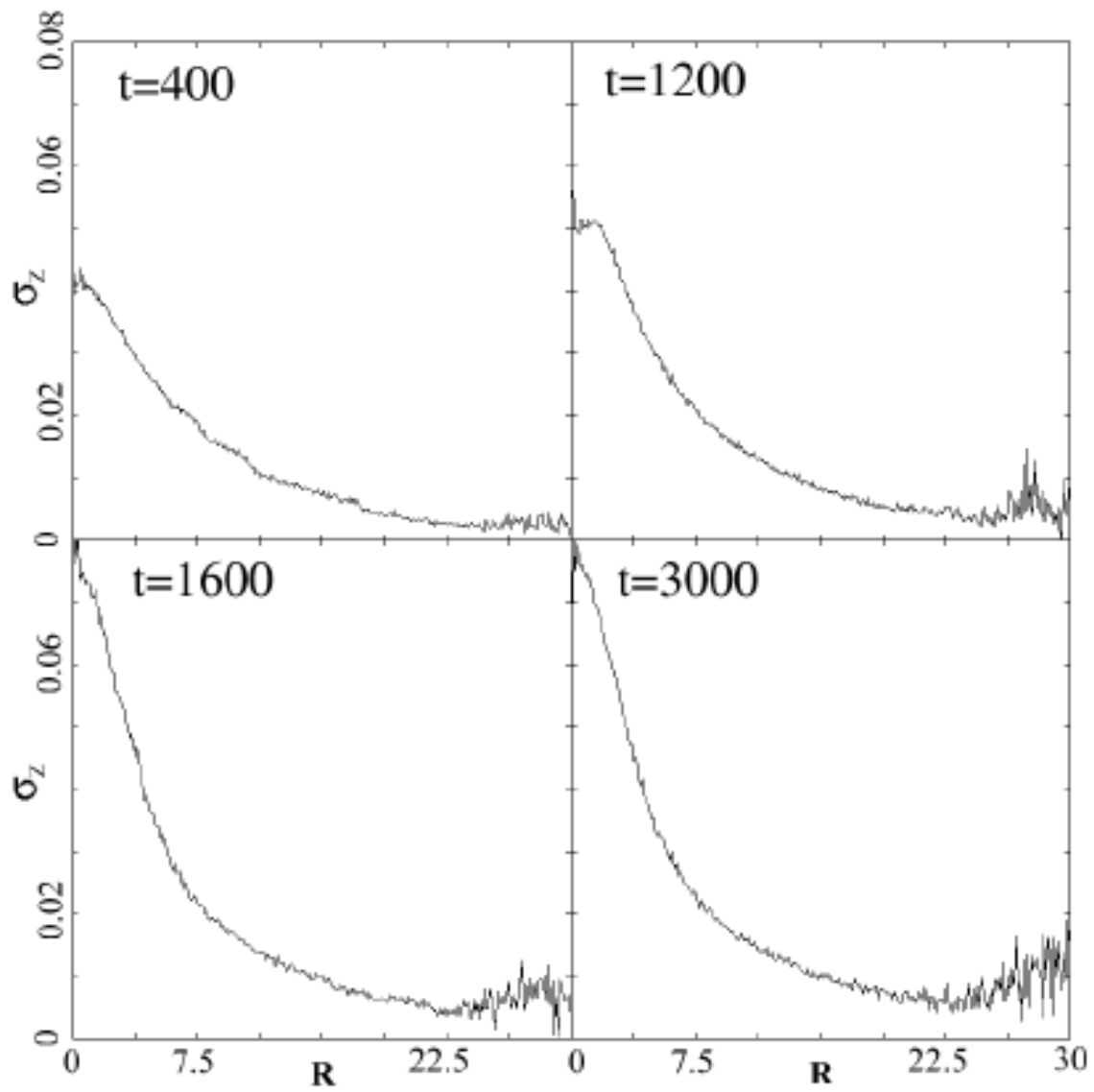
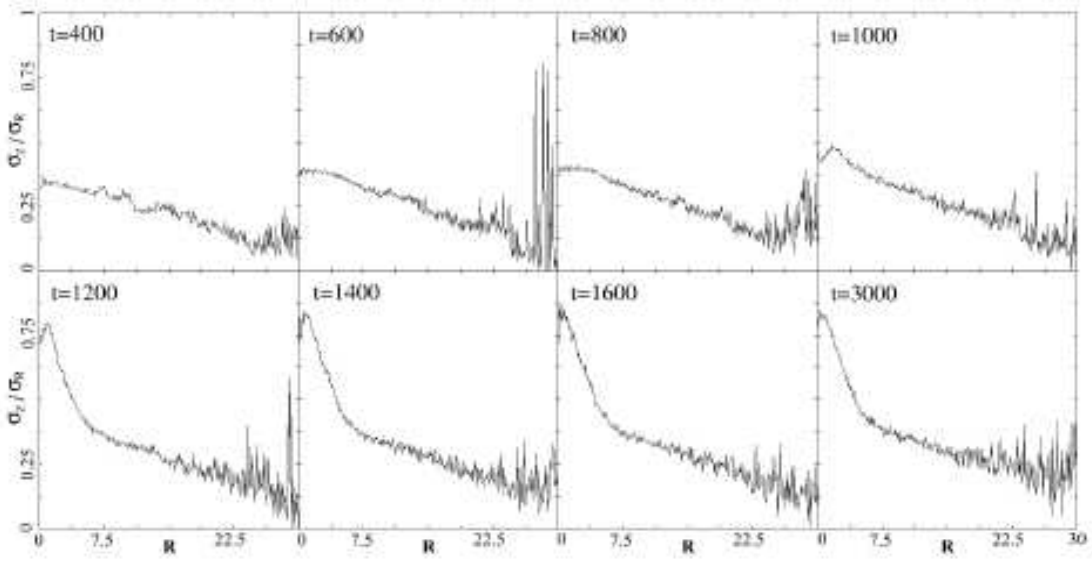


Figure 4: Model 26_1. σ_z versus R for several times.

26_1



8_1

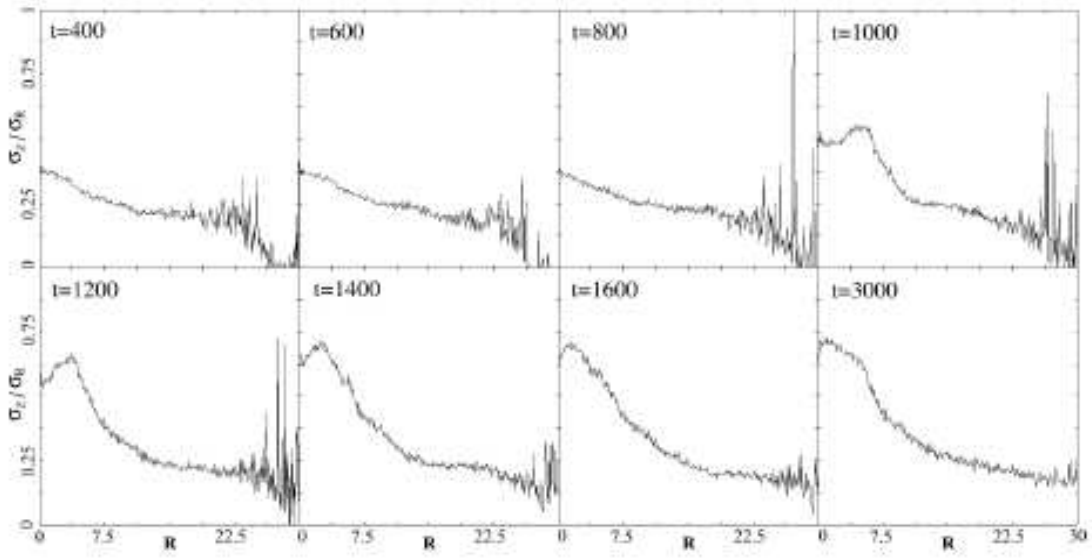


Figure 5: σ_z/σ_R versus R for several times: Models 26_1 and 8_1.

our numerical simulations and the theoretical calculations of Fridman and Polyachenko (1984) are inconsistent with the conclusions of Merrit and Sellwood (1994). These authors argue that the $m = 0$ mode is primarily stabilized in thick (radially hot) disks and the $m = 1$ mode must remain at the fore. In our numerical simulations, as the disk thickened, the growth rate of the $m = 0$ mode decreased sharply. A low-amplitude $m = 1$ mode was initially observed against the background of a slowly growing $m = 0$ mode; after the $m = 1$ mode displaced to the periphery, an axisymmetric bending clearly showed up. The vertical velocity dispersion in thick models began to increase only after the axisymmetric bending developed. Thus, for example, the disk bending in Model 32 was observed only 3000 Myr after the beginning of the evolution.

(4) In some of the models in which a bar was formed, only a small increase in the vertical velocity dispersion was associated with the initial bending of the entire disk. This applies to all of the models with $Q_{8.5} = 1.5$ and $z_0 < 0.3$ kpc. For thicker galaxies, no initial bending of the entire disk whatsoever was observed. In all of the models with $Q_{8.5} = 1.5$, the bending instability of the bar itself, which is investigated in the next subsection, was the leading heating mechanism.

The Bending Instability of Bars. The second vertical disk heating mechanism revealed by our numerical simulations is related to the bending instability of bars. A bar bending was first detected by Raha et al. in three-dimensional numerical simulations. Its appearance was explained by the development of firehose instability in the bar. In our simulations, this instability was responsible for the secular disk heating almost in all of the models with bars⁴.

Consider the disk evolution scenario using Model 8_1 as an example. The main evolutionary stages of the bending in this initially moderately hot model are shown in the color two-dimensional histograms (Fig. 6 and 7). At early stages ($t \approx 200 - 400$ Myr), the initial bending of the entire disk comes to the fore (the group of frames in the middle column). Gradually, the initial bending perturbation reaches its saturation level, is drifted to the galactic periphery, and decays ($t \approx 600$ Myr). A distinct bar has already been formed in the galaxy by this time (Figs. 6 and 7; the group of left frames; all images were oriented in such a way that the bar major axis was horizontal). At $t \approx 800$ Myr, the bending is generated already in the bar. At $t \approx 1000$ Myr, its amplitude reaches a maximum, after which the bending perturbation rapidly decays ($t \approx 1200 - 1600$ Myr).

The bar bending effect becomes understandable if we look at the group of right frames in Figs. 6 and 7. The shades of gray in these figures indicate the disk thickness in different disk regions. The thickness was calculated as $\sqrt{z^2(R, \varphi) - \overline{z(R, \varphi)}^2}$. We see that the bar was much thinner than the rest of the galaxy, which can be explained as follows. Since most of the disk stars were captured into the bar, it has a high surface density. Self-gravity causes the disk to become thinner in the bar region, which gives rise to a bending.

If we look at the plot of the vertical velocity dispersion against time (Fig. 3b), then

⁴In some of the models that started from $Q_{8.5} = 2.0$, despite the large velocity dispersion in the disk plane, a distinct bar was formed at late stages. However, by this time, the vertical velocity dispersion was so large (because of the relaxation associated with the bending instability of the entire disk) that no bending was formed in the bar.

we will see the curve rises twice: first at $t \approx 200$ Myr, which is clearly associated with the appearance of the initial bending of the entire disk, and, second, at $t \approx 1000 - 1200$ Myr, which coincides with the time the amplitude of the bar bending reaches its maximum.

In Fig. 5, σ_z/σ_R is plotted against R for several times. We see that for relatively cold disks (as in the case of hot disks; Fig. 5, Model 26_1), the general saturation level of the bending instability is higher than the linear level ((3). Merrit and Sellwood (1994) pointed out that moderately hot models ($Q \sim 1$) behave virtually as predicted by the linear theory. Large deviations take place only for hot models. In our simulations, we observed a similar picture. The saturation level of the bending instability associated with the entire disk in the models with $Q_{8.5} = 1.5$ is close to the linear level (see Fig. 5, $t = 800$, Model 8_1). However, when the bending instability of the forming bar came into effect, the final vertical disk heating was almost the same as that for the models with $Q_{8.5} = 2.0$ (see Fig. 5, $t = 3000$, Models 26_1 and 8_1).

For the remaining models with $Q_{8.5} = 1.5$ and a low dark-halo mass ($M_h(4h)/M_d(4h) < 1$), we observed the same growth stages of bending perturbations as those in Model 8_1. If a bar was formed in the disk, then bending instability sooner or later began to develop in it. The bending amplitude rapidly increased and the instability was ultimately saturated (all of these processes took place on time scales of the order of one billion years). Note that even the bending shape was in each case similar to that observed in Model 8_1. The models differed only by the bar formation time and by the duration of the stage that preceded the onset of bending formation in the bar itself. The larger was the dark-halo mass, the later the bar was formed and the farther was the time of bending generation in the bar from this time. The larger was the initial disk thickness, the later the bar was formed.

Stellar Relaxation in Models with a Massive Halo. Consider the stellar relaxation for models with a massive halo. A massive spherical component is known to effectively suppress the growth of bar-like instability (Ostriker and Peebles 1973) and to have a stabilizing effect on the growth of bending perturbations (Zasov et al. 1991; Sellwood 1996). The stellar relaxation in such models (if it takes place) must be produced by some other factors. Let us trace the evolution of the vertical structure of a stellar disk embedded in a massive halo using Model 9_1 as an example.

Because of the presence of a massive spheroidal component in the galaxy, the bending instability of its disk was suppressed. No bar was formed either (at least on a time scale of 5 Gyr). Since a massive halo primarily stabilizes the disk against the growth of perturbations in the disk plane with azimuthal numbers $m \leq 2$, higher-order modes come to the fore. They manifest themselves in the form of multiple shortlived spiral waves and persist in the disk for several disk rotations (see, e.g., the left frame in Fig. 8). Their amplitude is initially large but the spiral pattern is blurred almost completely by the time $t = 3000$ Myr.

Transient spirals are produced by collective processes and they are responsible for the heating of the disk in its plane. This relationship was first pointed out by Sellwood and Carlberg (1984). In Fig. 3c, the radial (σ_R) and vertical (σ_z) velocity dispersions are plotted against time. As would be expected, the rate of increase in the radial velocity dispersion slowly decreases with decreasing amplitude of the spiral arms and, after $t =$

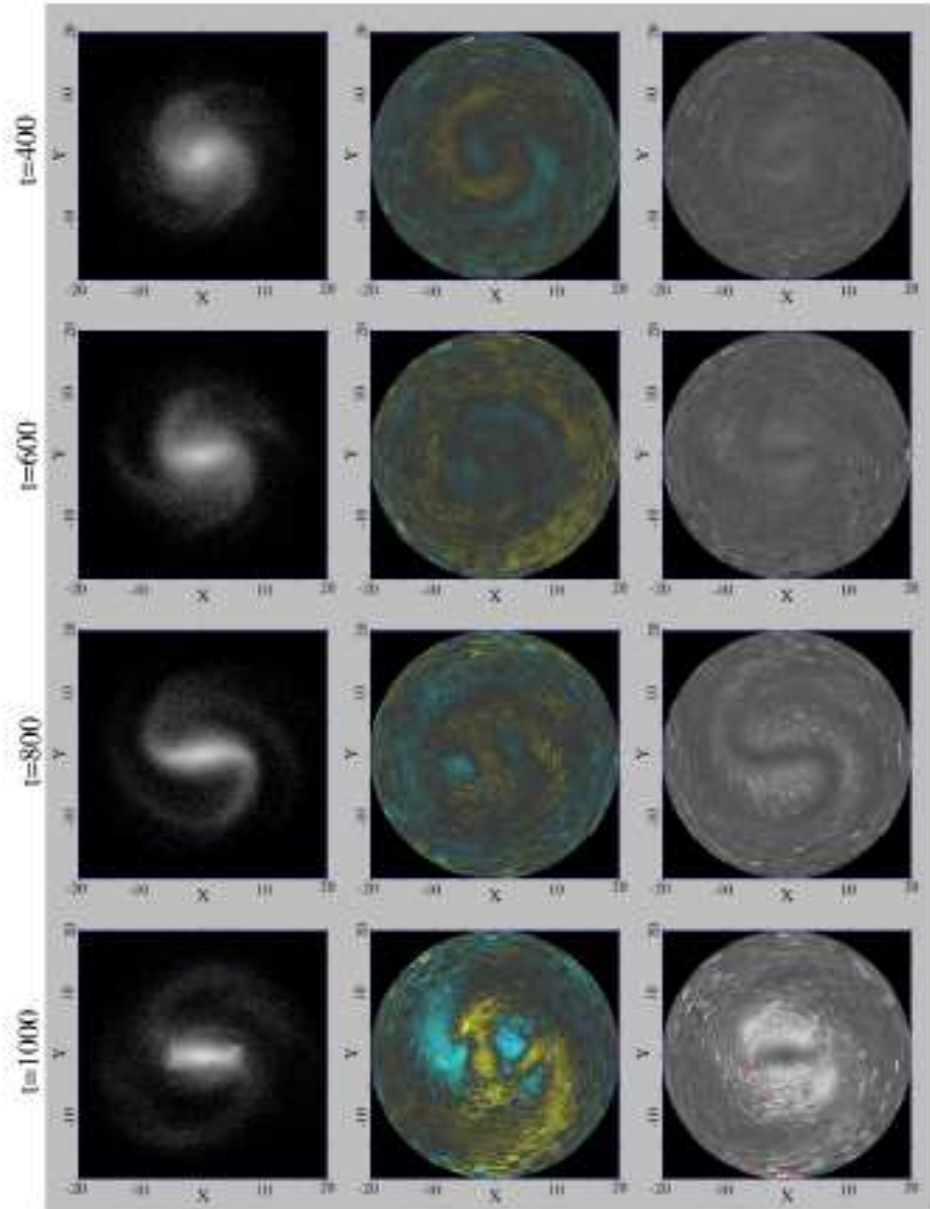


Figure 6: Model 8_1. The evolution of a disk with $Q_{8.5} = 1.5$ early stages). In each row: the first frame shows the galaxy seen face-on (the image brightness corresponds to the logarithm of the number of particles per pixel); the second frame shows the mean disk particle deviation from the $z = 0$ plane (this value is represented by different colors: the shades of yellow and blue indicate upward and downward deviations, respectively; the deviation ranges from -0.5 to $+0.5$ kpc); the third frame shows the two-dimensional galaxy thickness distribution (the thickness is indicated by the shades of gray: the lighter is the disk region, the thicker it is; the thickness ranges from 0 to 1 kpc; the red point means that the thickness in this region is outside the range). All pictures are oriented in such a way that the bar was located along the X axis. The frame size is $40 \text{ kpc} \times 40 \text{ kpc}$.

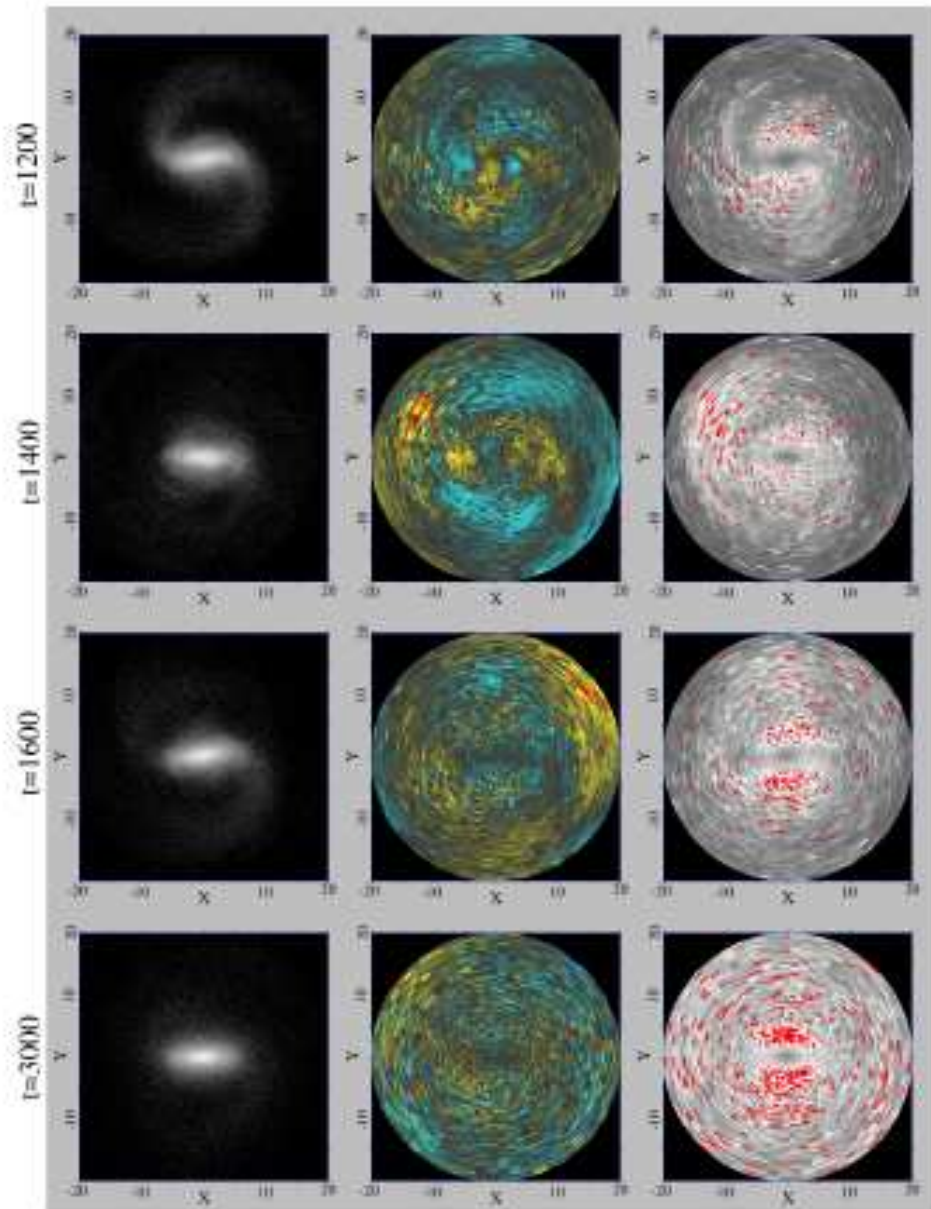


Figure 7: Model 8.1. The same as Fig. 6 for late evolutionary stages.

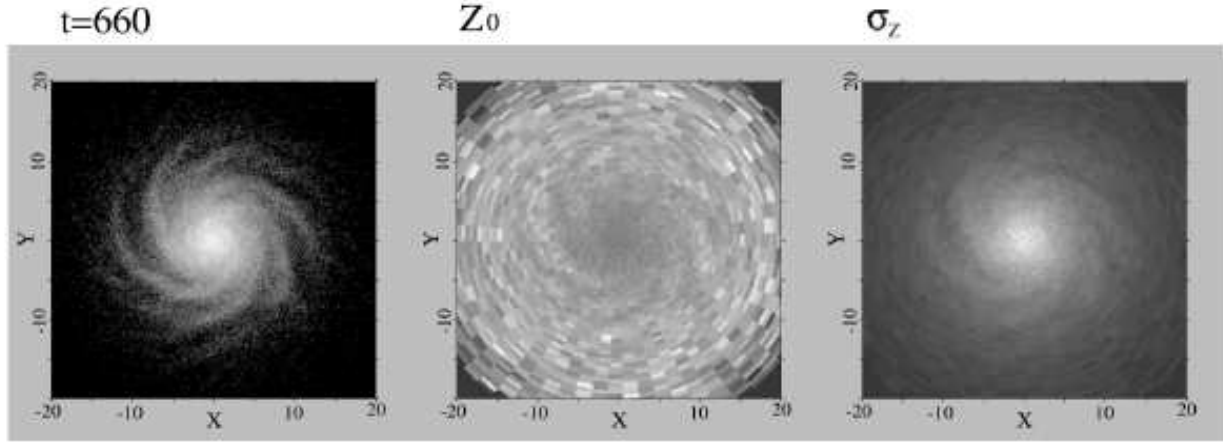


Figure 8: Model 9_1. A snapshot of the galaxy at $t = 660$ and the two-dimensional disk thickness and σ_z distributions. The size of each frame is 40×40 kpc. The left frame shows the galaxy seen face-on (the image brightness corresponds to the logarithm of the number of particles per pixel). The middle frame shows the two-dimensional disk thickness distribution constructed by using the shades of gray (the brighter the disk region, the larger its thickness at a given location). The right frame shows the two-dimensional σ_z distribution over the galaxy; σ_z is indicated by the shades of gray (the velocity dispersion is larger in brighter regions). We see that in the region of the spiral arms, the galaxy is thinner but the vertical velocity dispersion is larger. This effect is most pronounced for the two arms located in the lower right corner.

1500 Myr, the stellar relaxation in the disk plane related to transient spiral perturbations becomes ineffective. At the same time, for all five billion years of evolution, σ_z slowly increases, although the rate of increase gradually decreases. The observed vertical secular disk heating is not the result of numerical pair relaxation, because the levels and the patterns of increase of σ_z and σ_R differ greatly (σ_R is almost constant at late evolutionary stages). The cause of the increase of σ_z in our simulations is completely different.

Let us analyze the vertical disk structure in more detail. Figure 8 shows three frames for one of the times: the galaxy seen face-on, the two-dimensional disk thickness map, and the two-dimensional vertical velocity dispersion map. We clearly see from these frames that the disk thickness in the regions where the spiral arms are located is smaller than the disk thickness in the interarm space. In other words, inhomogeneities in the distribution of stars in the plane produce inhomogeneities in the vertical distribution of stars. The effect is similar in nature to the bar thinning described in the preceding section: a self-gravitating disk is thinner where the surface density is higher.

We assume that the observed increase of the vertical velocity dispersion is related to the scattering of stars by inhomogeneities in the distribution of matter in the z direction. Apart from the above explanation, there are two more additional facts that are indicative of this.

If we look at the two-dimensional σ_z distribution (Fig. 8), then we can see that σ_z in the spiral arms is higher than that in the interarm space. In addition, it follows from our computations that the decrease in the rate of increase of σ_z well correlates with the

decrease in the intensity of transient spirals.

Thus, we believe that the slow increase of the vertical velocity dispersion in our described models is attributable to the scattering of stars by transient spiral perturbations. The latter produce inhomogeneities in the vertical distribution of matter due to self-gravity.

Vertical Secular Disk Heating Mechanisms. During our numerical stellar-dynamics simulations, we scanned the space of control parameters (the initial disk half-thickness, the degree of disk heating in the disk plane, and the relative mass of the spheroidal subsystem). A detailed analysis of our numerical results revealed three distinct mechanisms of secular disk heating in the z direction.

- (1) The large-scale bending instability of the entire disk.
- (2) The bending instability of bars.
- (3) The heating due to inhomogeneities in the vertical distribution of stars produced by matter inhomogeneities in the plane.

The action of a particular heating mechanism depends on the control parameters. If the bar mode is suppressed in the galaxy, then the heating is attributable to the large-scale bending instability associated with the entire disk. This is the case of a hot disk ($Q_{8.5} > 1.5$) and (or) a moderately massive halo. In this case, the heating of the central regions is particularly strong. The saturation level of the bending instability in these regions is almost a factor of 2.5 higher than the level that follows from the linear theory. The bending mode with the azimuthal number $m = 0$ plays a key role in the secular heating. The time of its occurrence depends on the initial disk thickness: the thicker is the disk, the farther in time is the secondary rise in disk temperature related to the growth of the bell mode.

If a bar mode develops in the disk, then the bending instability of the bar gives the largest contribution to the heating. Until a bar is formed, the maximum value of σ_z/σ_R is 0.37 in the central regions and 0.3 on the periphery. This is the level that the bending instability associated with the entire disk reaches. It is in good agreement with the linear criterion. After the formation of a bar, at the time of its bending in the central regions, σ_z/σ_R rises to 0.7 – 0.8. The heating on vertical bar bending perturbations dominates in initially moderately hot disks ($Q_{8.5} = 1.5$) with a low-mass halo.

The heating on vertical inhomogeneities take place when the bending modes and the bar mode were suppressed. This was observed for moderately hot models ($Q_{8.5} = 1.5$) with a massive halo. Note that the secular disk heating in all directions in similar simulations has been observed more than once. However, we are probably the first to associate the increase of σ_z with the scattering of stars by vertical inhomogeneities.

CONCLUSIONS

We have numerically analyzed the nonlinear growth stages of bending instability in stellar disks with exponential radial density profiles and found significant deviations from the linear theory.

- (1) All of the observed modes are global; i.e., the scale of unstable perturbations is larger than the typical scale of density variations in the disk. Our conclusion agrees

with the conclusions of Sellwood (1996). It implies that, although the dispersion relation (1) derived for a homogeneous layer is also locally valid for inhomogeneous disks (in particular, exponential disks, as in our numerical simulations), it would be inappropriate to use this relation to analyze the saturation level of long-wavelength perturbations. This also suggests that bending instability will develop in inhomogeneous disks differently in different parts of the galaxy.

(2) The value of $(\sigma_z/\sigma_R)_{\text{cr}} \approx 0.3$ was obtained from a linear analysis. As our numerical computations show, the saturation level of large-scale bending perturbations is a factor of 2 or 3 higher than the linear level. The differences are best seen in central regions of the stellar disk. The lower the dark-halo mass, the higher the instability saturation level and the larger the ratio of the vertical and radial velocity dispersions averaged within two exponential disk scale lengths. A similar dependence was pointed out by Mikhailova et al. (2001), although without discussing the underlying mechanisms. Early-type spiral galaxies have, on average, a smaller dark-to-luminous mass ratio and, as follows from the observational data given above, a larger value of σ_z/σ_R , in agreement with our computations.

(3) The instability saturation time scales are several billion years.

(4) Our numerical simulations revealed three distinct mechanisms of the secular heating of stellar disks in the z direction. We confirmed the existence of bar bending instability that was first detected by Raha et al. (1991). For a large series of models, we showed that the bar bending is an inevitable stage of its evolution.

Thus, we can conclude that bending instability can play an important role in the secular disk heating in the z direction.

ACKNOWLEDGMENTS

This work was supported in part by the Program “Leading Scientific Schools” (project no. 00-15-96607), the Federal Program “Astronomy” (project no. 40.022.1.1.1101), and the UR grant no. 02.01.006.

REFERENCES

- [1] *S. Araki*, Ph.D. Thesis, Massachus. Inst. Tech. (1985).
- [2] *J. Barnes and P. Hut*, Nature 324, 446 (1986).
- [3] *J. Binney and C. Lacey*, Mon. Not. R. Astron. Soc. 230, 597 (1988).
- [4] *J. Binney and S. Tremaine*, Galactic Dynamics (Princeton University, 1987).
- [5] *J. Binney, W. Dehnen, and G. Bertelli*, Mon. Not. R. Astron. Soc. 318, 658 (2000).
- [6] *H. Velazquez and S. D.M. White*, Mon. Not. R. Astron. Soc. 304, 254 (1999).

- [7] *J. Gerssen, K. Kuijken, and M. Merrield*, *Mon. Not. R. Astron. Soc.* 288, 618 (1997).
- [8] *J. Gerssen, K. Kuijken, and M. Merrield*, *Mon. Not. R. Astron. Soc.* 317, 545 (2000).
- [9] *W. Dehnen and J. J. Binney*, *Mon. Not. R. Astron. Soc.* 298, 387 (1998).
- [10] *A. Jenkins*, *Mon. Not. R. Astron. Soc.* 257, 620 (1992).
- [11] *A. Jenkins and J. Binney*, *Mon. Not. R. Astron. Soc.* 245, 305 (1990).
- [12] *A. V. Zasov, D. I. Makarov, and E. A. Mikhailova*, *Pis'ma Astron. Zh.* 17, 884 (1991) [*Sov. Astron. Lett.* 17, 374 (1991)].
- [13] *R. M. Kulsrud, J.W.-K.Mark, and A. Caruso*, *Astrophys. Space Sci.* 14, 52 (1971).
- [14] *F. Combes, F. Debbasch, D. Friedli, and D. Pfenninger*, *Astron. Astrophys.* 233, 82 (1990).
- [15] *C. G. Lacey*, *Mon. Not. R. Astron. Soc.* 208, 687 (1984).
- [16] *D. Merrit and J. A. Sellwood*, *Astrophys. J.* 425, 551 (1994).
- [17] *M. Merrifield, J. Gerssen, and K. Kuijken*, *Astron. Soc. Pac. Conf. Ser.* 230, 221 (2001).
- [18] *E. A. Mikhailova, A. V. Khoperskov, and S. S. Sharpak*, in *Stellar Dynamics — from Classic to Modern*, Ed. by L. P. Ossipkov and I. I. Nikiforov, (St.-Peterburg Gos. Univ., St. Petersburg, 2001), p. 147.
- [19] *J. P. Ostriker and P. J.E. Peebles*, *Astrophys. J.* 186, 467 (1973).
- [20] *P. P. Parenago*, *Astron. Zh.* 27, 150 (1950).
- [21] *P. A. Patsis, E. Athanassoula, P. Grosbol, and Ch. Skokos*, *Mon. Not. R. Astron. Soc.* 335, 1049 (2002).
- [22] *V. L. Polyachenko and I. G. Shukhman*, *Pis'ma Astron. Zh.* 3, 254 (1977) [*Sov. Astron. Lett.* 3, 134 (1977)].
- [23] *D. Pfenninger and D. Friedli*, *Astron. Astrophys.* 252, 75 (1991).
- [24] *N.Raha, J. A.Sellwood, R. A. James, and F.D.Kahn*, *Nature* 352, 411 (1991).
- [25] *V. Reshetnikov and F. Combes*, *Astron. Astrophys.* 324, 80 (1997).
- [26] *W. C. Saslaw*, *Gravitational Physics of Stellar and Galactic Systems* (Cambridge Univ. Press, Cambridge, 1985).
- [27] *J. A. Sellwood*, *Astrophys. J.* 473, 733 (1996).

- [28] *J. A. Sellwood and R. G. Carlberg*, *Astrophys. J.* 282, 61 (1984).
- [29] *J. A. Sellwood and D. Merritt*, *Astrophys. J.* 425, 530 (1994).
- [30] *L. Spitzer and M. Schwarzschild*, *Astrophys. J.* 114, 385 (1951).
- [31] *L. Spitzer and M. Schwarzschild*, *Astrophys. J.* 118, 106 (1953).
- [32] *P. J. Teuben*, *Astron. Soc. Pac. Conf. Ser.* 77, 398 (1995).
- [33] *A. Toomre*, *Astrophys. J.* 139, 1217 (1964).
- [34] *A. Toomre*, *Geophys. Fluid Dyn.* no. 66-46, 111 (1966).
- [35] *I. W. Walker, J. Ch. Mihos, and L. Hernquist*, *Astrophys. J.* 460, 121 (1999).
- [36] *A. M. Fridman and V. L. Polyachenko*, *Physics of Gravitating Systems* (Springer-Verlag, New York, 1984).
- [37] *B. Fuchs, C. Dettbarn, H. Jahreis, and R. Wielen*, *Astron. Soc. Pac. Conf. Ser.* 228, 235 (2000).
- [38] *C. Hunter and A. Toomre*, *Astrophys. J.* 155, 747 (1969).
- [39] *L. Hernquist*, *Astrophys. J. Suppl. Ser.* 64, 715 (1987).
- [40] *L. Hernquist*, *Astrophys. J. Suppl. Ser.* 86, 389 (1993).

Translated by V. Astakhov